




Critical current density of $(\text{Bi}_{1.6}\text{Pb}_{0.4})\text{Sr}_2\text{Ca}_2\text{Cu}_3\text{O}_{10}$ superconductor irradiated with neutron in in-core facilities: rotary rack and dry tube at PUSPATI TRIGA Research Reactor

Madiah Mujaini^{1,2,3} · A. B. P. Ilhamsyah^{1,2,3} · K. Muhammad-Najib³ · Nasri A. Hamid¹ · Rozidawati Awang³ · Faridah Mohamad Idris⁴ · Abi Muttaqin Jalal Bayar⁴ · Na'im Syauqi Hamzah⁴ · R. Abd-Shukor³ 

Received: 23 January 2023 / Accepted: 22 March 2023 / Published online: 31 March 2023
© The Author(s), under exclusive licence to Springer-Verlag GmbH, DE part of Springer Nature 2023

Abstract

The effects of neutron irradiation in dry tube (DT) and rotary rack (RR) facilities at PUSPATI TRIGA Reactor on the superconducting properties of $(\text{Bi}_{1.6}\text{Pb}_{0.4})\text{Sr}_2\text{Ca}_2\text{Cu}_3\text{O}_{10}$ (Bi-2223) are reported. The samples were prepared via the co-precipitation method and exposed to neutron irradiation in both facilities for 0.25 h to 5 h with neutron flux 6.90×10^{12} and 2.75×10^{12} $\text{n cm}^{-2} \text{s}^{-1}$, respectively. The structure, microstructure, radionuclide, electrical resistance, and AC susceptibility were determined. Energy-dispersive X-ray analysis revealed the presence of Zn and Po due to the neutron activation. Gamma spectroscopy analysis showed that neutron irradiation produced ^{85}Sr radionuclide. The electrical resistance showed onset temperature, $T_{c\text{-onset}}$ of 118 K and transport critical current density, $J_{c\text{-t}}$ of 2.14 A cm^{-2} at 50 K for the non-irradiated sample. AC susceptibility showed that the transition temperature, $T_{c\chi}$ was around 106 to 109 K and 105 to 109 K for samples irradiated in DT and RR facilities, respectively. The lower peak temperature, T_{pL} of the imaginary part of the susceptibility, χ'' varied from 88 to 97 K. Sample irradiated for 4 h with neutron fluence of 3.96×10^{16} n cm^{-2} in RR facility showed the highest $J_{c\text{-t}}$ (15.88 A cm^{-2} at 50 K). Samples irradiated in RR showed higher $J_{c\text{-t}}$ compared with samples irradiated in DT facility. Neutron irradiation suppressed the transition temperature and Bi-2223 phase, but improved $J_{c\text{-t}}$ by more than six times in DT and seven times in RR facility. The optimal neutron fluence for neutron irradiation in Bi-2223 was between 2.48×10^{16} and 3.96×10^{16} n cm^{-2} .

Keywords AC susceptibility · Critical current density · Dry tube · Rotary rack

1 Introduction

The Bi–Sr–Ca–Cu–O (BSCCO) superconductor is a cuprate-based high-temperature superconductor (HTS) that has received a lot of attention due to the stability of the

superconducting phase, a relatively high transition temperature, T_c and critical current density, J_c . The general formula is $\text{Bi}_2\text{Sr}_2\text{Ca}_{n-1}\text{Cu}_n\text{O}_{2n+4+y}$ where $n = 1, 2$ and 3 refers to the number of CuO_2 layers. The BSCCO superconductors consist of single, double, and triples layers of CuO_2 and are known as Bi-2201, Bi-2212, and Bi-2223 phases which superconduct at 20, 81, and 110 K, respectively.

A considerable amount of works have been reported on the preparation, superconducting properties, and structure of the Bi-2223 phase, which has the highest transition temperature, T_c among the BSCCO family. Substitution of Pb at Bi site improved T_c [1] and high Bi-2223 phase. Sample prepared the by co-precipitation method also produces a high-quality superconductor [2]. Besides that, the addition of magnetic and non-magnetic nanoparticles such as $\text{Ni}_{0.5}\text{Zn}_{0.5}\text{Fe}_2\text{O}_4$ [3], NiFe_2O_4 [4], PbS [5], Fe_2O_3 [6] and NiO [7] enhanced J_c of Bi-2223. The addition of magnetic nanoparticles with size, d between the coherence length, ξ

✉ R. Abd-Shukor
ras@ukm.edu.my

¹ College of Engineering, Universiti Tenaga Nasional, Jalan IKRAM-UNITEN, 43000 Kajang, Selangor, Malaysia

² Institute of Sustainable Energy, Universiti Tenaga Nasional, Jalan IKRAM-UNITEN, 43000 Kajang, Selangor, Malaysia

³ Department of Applied Physics, Universiti Kebangsaan Malaysia, 43600 Bangi, Selangor, Malaysia

⁴ Reactor Technology Centre, Technical Support Division, Malaysian Nuclear Agency, 43000 Kajang, Selangor, Malaysia

and penetration depth, λ ($\xi < d < \lambda$) can increase J_c [8]. An effective flux pinning can be achieved if the size of the defect is within the coherence length [9].

Neutron irradiation is another method to improve the flux pinning capability as well as optimizing the hole concentration of Bi-2223 phase. This is due to the ability of neutron irradiation to induce point defects which can cascade into the microstructure and possibly increase T_c and J_c [10]. Besides that, the elastic collision between neutrons and atoms generates many defects mainly due to the oxygen atom. Oxygen atoms are the major mobile element in the BSCCO system, and therefore, oxygen atoms move from their ideal sites through incident neutrons transfer energy. These oxygen atoms movements generate a large number of vacancies and interstitial oxygen atoms that can modify the hole concentration [11]. Furthermore, neutron irradiation can introduce defect clusters of several nanometer in all parts of the samples isotropically [12].

Several studies showed that neutron irradiated Bi-2223 samples exhibit improved flux pinning capability and substantially increased J_c . Irradiation with lower neutrons fluence (10^3 n cm⁻²) enhanced superconducting properties better than higher neutron fluence (10^{17} n cm⁻²) [13]. Bi-2223/Ag sheathed tapes irradiated with neutron showed significant improvement in J_c at higher fields [14]. Fast neutron irradiation does not suppress the superconducting properties of Bi-2223 tapes and radioactive isotope analysis showed that the tape is safe to be used in medical accelerators [15]. The distribution of the pinning energy for neutron irradiation increased remarkably when compared to electron irradiation [16]. Magnetization studies on neutron irradiated Bi-2223 revealed that at a higher fluence (8.0×10^{16} n cm⁻²), the critical magnetic field, H_c , and penetration depth in the a - b plane, λ_{ab} increased by 30% and 15%, respectively [17]. Neutron irradiated uranium doped Bi-2223 increased the number of flux pinning center compared with undoped Bi-2223 samples [18].

The Malaysian's PUSPATI TRIGA Reactor (RTP) has achieved its initial criticality on 28 June 1982 and is equipped with several irradiation facilities in the core and outside the core of reactor for research purposes. Among the in-core facilities are rotary rack (RR) and dry tube (DT) as shown in Fig. 1. The rotary rack facility is located around the top portion of the core and inside the graphite reflector. The rotary rack assembly is made up of a ring-shaped, seal-welded aluminum housing that contains an aluminum rack that is mounted on special bearings [19]. It supports 40 uniformly spaced tubular aluminum storages that hold the specimen containers. The dry tube facility consists of empty tube located in core position in the reactor. The RR facility is a rotating system while DT facility is a non-rotating system. Thus, it is expected that the neutron fluence in RR facility is more uniform than DT facility. Studies on neutron

flux distribution showed that the dry tube facility exhibited higher neutron flux compared with the rotary rack facility [20]. The thermal, epithermal and fast neutron fluxes for DT are 6.90×10^{12} , 4.51×10^{12} and 5.33×10^{12} n cm⁻² s⁻¹, respectively, while for RR is 2.75×10^{12} , 1.15×10^{12} and 8.61×10^{11} n cm⁻² s⁻¹, respectively [20]. It is interesting to compare the effect of neutron irradiation in DT and RR facilities on the superconducting properties of (Bi_{1.6}Pb_{0.4})Sr₂Ca₂Cu₃O₁₀ superconductor. Hence, the objective of this study was to investigate the effect of neutron irradiation in dry tube (higher neutron flux) and rotary rack (lower neutron flux) facilities with different neutron fluences on the superconductivity of Bi-2223 superconductor. Another objective of this study was to investigate the effect of non-rotating (DT facility) and rotating (RR facility) systems on the neutron flux distribution on Bi-2223 superconductor.

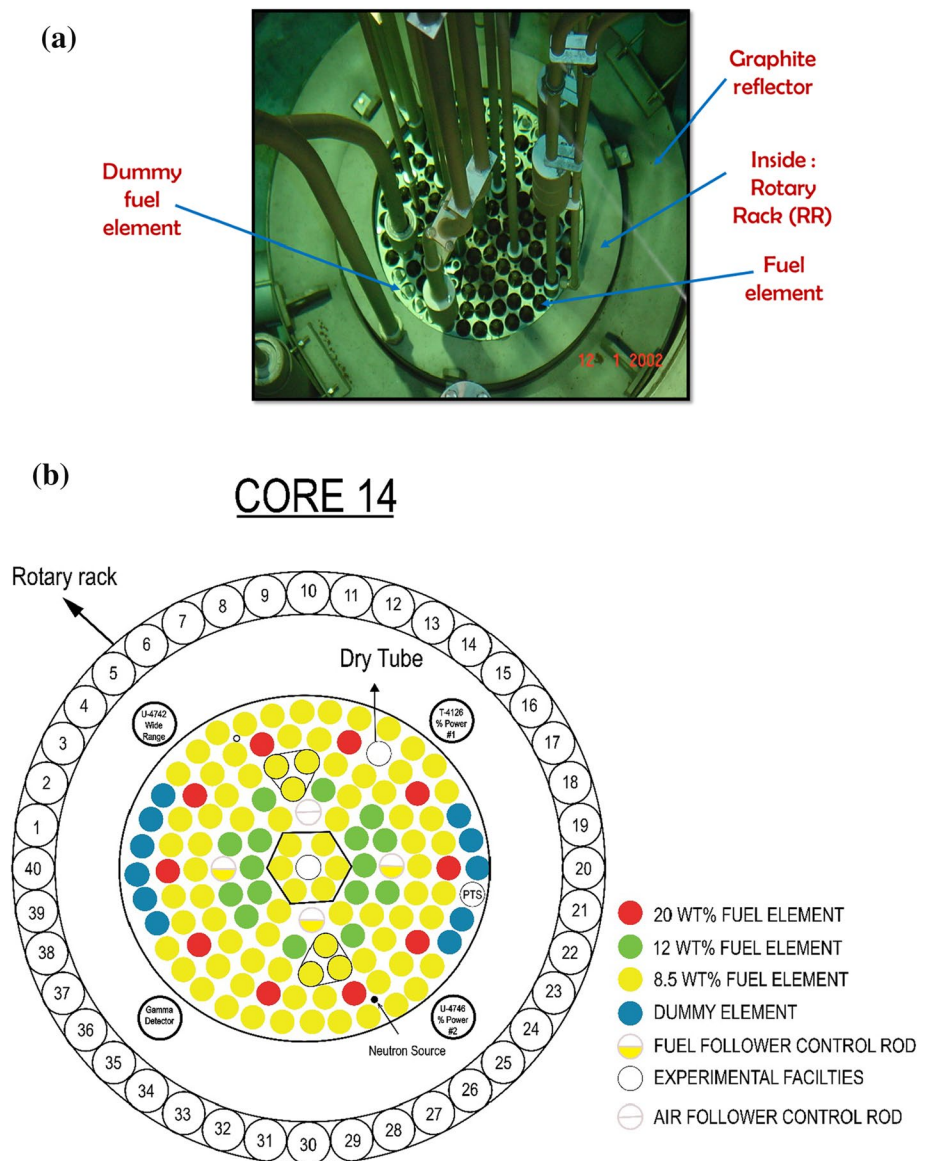
In this study, (Bi_{1.6}Pb_{0.4})Sr₂Ca₂Cu₃O₁₀ samples were exposed to neutron flux of 6.90×10^{12} and 2.75×10^{12} n cm⁻² s⁻¹ in DT and RR facilities, respectively for 0.25, 0.50, 0.75, 1.00, 2.00, 3.00, 4.00 and 5.00 h. The X-ray diffraction (XRD) method was used to determine the resultant phase. The radionuclides were determined by neutron activation and scattering calculator and gamma spectroscopy. The electrical resistance and AC susceptibility were measured along with the microstructural properties.

2 Experimental details

The size of starting superconductor powders is one of the parameters that must be considered to produce a high quality superconductor. In this work, the fine superconductor powders produced by the co-precipitation method were used to prepare (Bi_{1.6}Pb_{0.4})Sr₂Ca₂Cu₃O₁₀. High purity ($\geq 99.99\%$) bismuth acetates, strontium acetates, lead acetates, calcium acetates, copper acetates, and oxalic acid were used as starting components. The acetates were weighed stoichiometrically and dissolved in the optimum amount of acetic acid (solution A). The oxalic acid was dissolved in deionized water: isopropanol (1:1.5) to have a concentration of 0.5 M at 0 to 2 °C (solution B). Solution B was added to solution A in an ice bath where a uniform, stable, blue suspension was obtained. The slurry was filtered using a vacuum filter after a navy blue slurry was formed. The navy-blue precipitate was dried at 80 °C overnight. The navy-blue precipitate precursor powders were pre-heated at 730 °C in air for 12 h. The pre-heated powders were reground and heated again at 850 °C in air for 24 h and furnace cooled. The powders were reground and then pressed into pellets with 12.5 mm diameter and 3 mm thickness. The pellets were sintered at 850 °C for 48 h followed by furnace cooling.

Several samples were irradiated with neutrons in DT and RR facilities at PUSPATI TRIGA Research Reactor. The DT

Fig. 1 **a** Rotary rack and **b** dry tube position in PUSPATI TRIGA Research Reactor at Malaysia Nuclear Agency



facility is located at one of the in-core positions in the reactor while the RR facility is located at the top portion of the core inside the graphite reflector and contains 40 irradiation positions as shown in Fig. 1. The samples were sealed in a container before being put inside the facilities. Special hook rods were used to insert and remove samples from DT and RR facilities. The energies of neutrons range from 1 eV to 10 MeV, with thermal neutrons ($E_{\text{kin}} < 1.0$ eV) accounting for 41% and 58% of the neutron energy spectrum in DT and RR facilities, respectively [20, 21]. Hence, all fluences in this work are referred to thermal neutrons. The samples were irradiated in DT and RR facilities with thermal neutron flux 6.90×10^{12} and 2.75×10^{12} $\text{n cm}^{-2} \text{s}^{-1}$ for 0.25, 0.50, 0.75, 1.00, 2.00, 3.00, 4.00 and 5.00 h. The corresponding thermal neutron fluences captured by the samples in DT facility were 6.21×10^{15} , 1.24×10^{16} , 1.86×10^{16} , 2.48×10^{16} , 4.97×10^{16} ,

7.45×10^{16} , 9.94×10^{16} and 1.24×10^{17} n cm^{-2} . In RR facility, the corresponding neutron fluences were 2.48×10^{15} , 4.95×10^{15} , 7.43×10^{15} , 9.90×10^{15} , 1.98×10^{16} , 2.97×10^{16} , 3.96×10^{16} and 4.95×10^{16} n cm^{-2} . The samples were left in the chamber for a month after radiation to reduce the activity to a safe level.

The phase was identified by X-ray powder diffraction (XRD) method using a Bruker D8 Advance diffractometer with $\text{CuK}\alpha$ source. A PDF (00-042-0415) from ICDD data bank was used as a reference for the $(\text{Bi}_{1.6}\text{Pb}_{0.4})\text{Sr}_2\text{Ca}_2\text{Cu}_3\text{O}_{10}$ (Bi-2223) phase. The lattice parameters were calculated using the Xpert High Score software. The volume fraction for the phases was determined by using the ratio of the sum of the intensities of all phases.

Field emission scanning electron microscope (FESEM) micrographs were observed using a Merlin Gemini scanning

electron microscope. Energy-dispersive X-ray analysis (EDX) with Oxford Instrument analyzer were used to determine the elemental composition of the samples. The neutron activation of elements was estimated by Neutron Activation and Scattering Calculator.

Radionuclide detection was performed by gamma spectrometer using an ORTEC coaxial high purity germanium (HPGe) detector. The sample counting time was 28,800 s. A multi-channel analyzer (MCA) and Gamma Vison Analysis software were used to analyze the peak energy in gamma spectra.

The temperature-dependent electrical resistance measurements were conducted using the four-probe method with silver paste contacts. The samples were cut into bar shaped with dimensions of approximately 13 mm × 2 mm and average distance between contact was about ~ 2 mm. The setup consisted of a Keithley 197 Microvolt Digital Multimeter and Keithley 220 Current Source. A closed cycle refrigerator from CTI Cryogenics Model 22 and a temperature controller from Lake Shore Cryotronics Model 325 were used for electrical resistance–temperature measurements. The transport critical current density, J_{c-t} was determined using the 1 μ V/cm criterion from 50 to 77 K.

An AC susceptometer from Cryo Industry model number REF-1808-ACS was used to measure the susceptibility. The samples were cut into bar shape for the measurement. The frequency of the AC signal used was 295 Hz and the magnetic field was $H = 5$ Oe.

3 Results and discussion

This section presents the results of XRD patterns, microstructure, radionuclide analysis, electrical resistance, AC susceptibility and critical current density measurements.

3.1 XRD patterns

Figure 2a, b show the XRD patterns of non-irradiated ($\text{Bi}_{1.6}\text{Pb}_{0.4}\text{Sr}_2\text{Ca}_2\text{Cu}_3\text{O}_{10}$) and samples irradiated in DT facility for 0.25, 0.50, 0.75, 1.00, 2.00, 3.00, 4.00 and 5.00 h. XRD patterns revealed the presence of Bi-2223 and Bi-2212 phase in all samples. The volume fraction of Bi-2223 phase with tetragonal unit cell was the highest for non-irradiated sample. All irradiated samples exhibited a lower volume fraction of Bi-2223 phase compared with non-irradiated sample and generally showed nearly 50:50 ratio of the Bi-2212: Bi-2223 phase. The lattice parameters for the non-substituted sample were $a = 5.406$ Å and $c = 37.134$ Å. Peaks due to Bi-2201 phase were also observed in the non-irradiated sample and samples irradiated for 0.25 and 2.00 h. The Bi-2201 phase was denoted by (*).

XRD patterns of samples irradiated in RR facility for 0.25, 0.50, 0.75, 1.00, 2.00, 3.00, 4.00 and 5.00 h are shown in Fig. 3. The Bi-2223 phase was dominant for all samples except for samples irradiated for 0.25, 0.75, and 5.00 h. However, the volume fraction of Bi-2223 phase was suppressed for all irradiated samples. Sample irradiated for 5.00 h with equivalent to 4.95×10^{16} n cm^{-2} fluence showed the highest volume fraction of Bi-2212 phase. The samples irradiated for 2.00 and 4.00 h revealed the formation of Bi-2201 phase.

The XRD patterns demonstrated that all irradiated samples in both DT and RR facilities reduced the Bi-2223 phase. In general, samples irradiated in DT facility severely reduced the Bi-2223 phase compared with samples irradiated in RR facility. Several samples in DT (0.25 and 2.00 h) and RR (2.00 and 4.00 h) facilities showed the existence of Bi-2201 phase. Neutron irradiation induced atomic displacement that caused disorder in Cu–O chain and intergrowth of CuO_2 planes, which resulted in the formation of multiphases in the sample [22]. Our results showed the formation of Bi-2212 phase was increased after irradiation, but the formation of Bi-2201 phase was greatly suppressed, with no peak observed in the XRD pattern for almost all samples. This suggested that the neutron irradiation induced point defect (atomic displacement) that promoted the formation of Bi-2212 phase but hindered the Bi-2201 phase formation. There was no systematic change in lattice parameters and volume of unit cell for all irradiated samples. This was due to crystalline lattice distortion and atom displacement initiated by neutron irradiation led to cluster defects and the concentration of overlapping defects upon irradiation [11].

3.2 FESEM micrographs

FESEM micrographs for (a) non-irradiated sample, sample irradiated for (b) 2 h in DT facility and (c) 2 h in RR facility are shown in Fig. 4. FESEM micrographs showed platelet-like microstructures that were randomly oriented in all samples. Several layers of the superconducting grains packed together in well-ordered manner were observed in all samples. Samples irradiated for 2 h in RR facility showed a smaller grain size with higher porosity compared with non-irradiated sample and sample irradiated for 2 h in DT facility.

3.3 EDX analyses

Figure 5 shows the EDX spectra with elemental atomic and weight percent for (a) non-irradiated sample, (b) sample irradiated for 2 h in DT facility and (c) sample irradiated for 2 h in RR facility. Peaks corresponding to Bi, Pb, Sr, Ca, Cu and O elements were observed in all samples. There were slight variations in the ratio of atomic and

Fig. 2 XRD patterns of non-irradiated $(\text{Bi}_{1.6}\text{Pb}_{0.4})\text{Sr}_2\text{Ca}_2\text{Cu}_3\text{O}_{10}$ and samples irradiated in DT facility for 0.25, 0.50, 0.75, 1.00, 2.00, 3.00, 4.00 and 5.00 h. Peaks with parenthesis and (*) indicate the Bi-2212 and Bi-2201 peaks, respectively

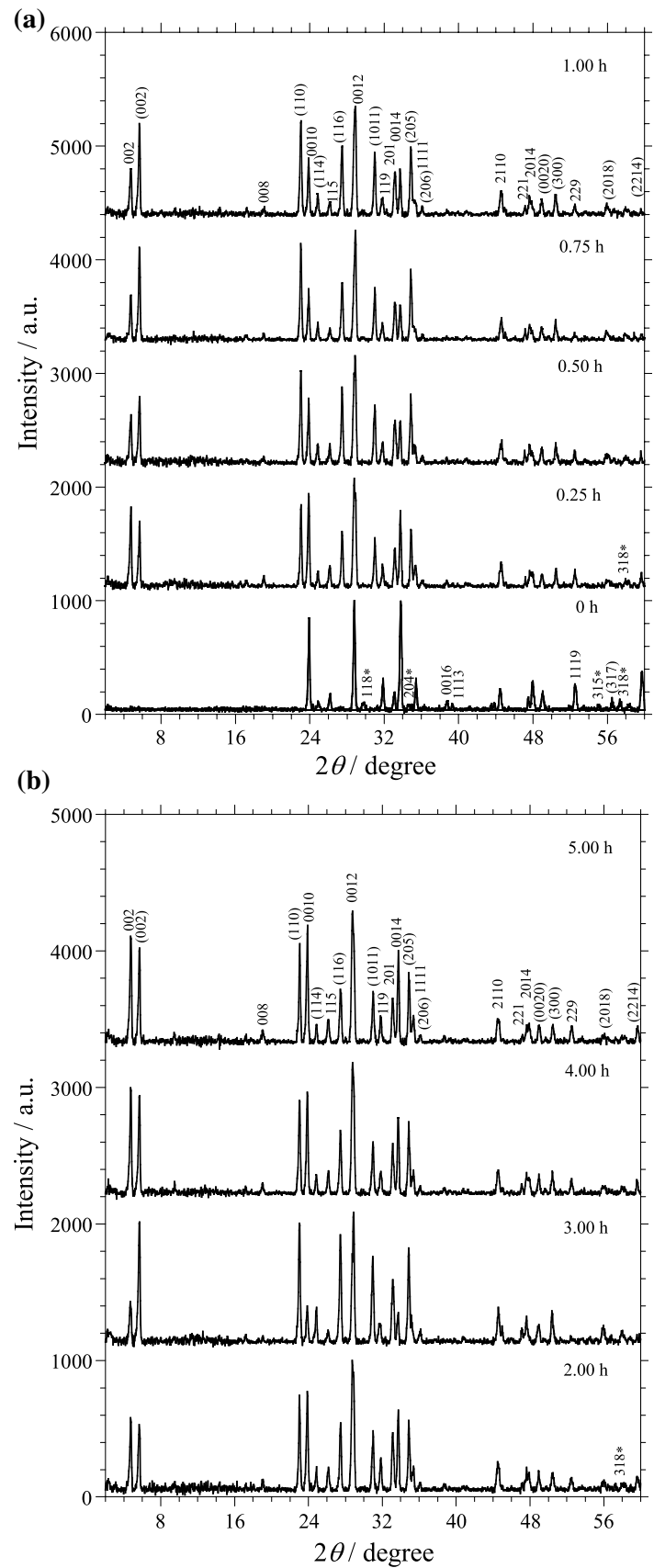
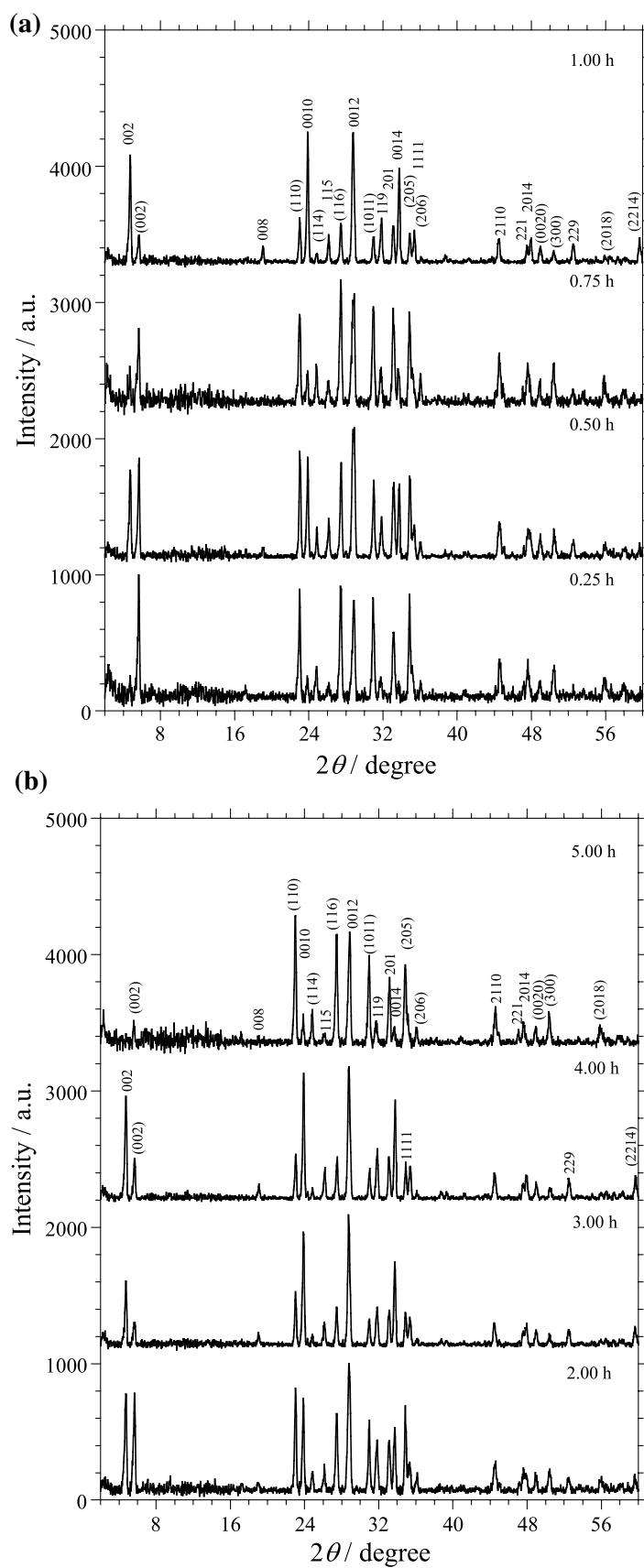


Fig. 3 XRD patterns of $(\text{Bi}_{1.6}\text{Pb}_{0.4})\text{Sr}_2\text{Ca}_2\text{Cu}_3\text{O}_{10}$ irradiated in RR facility for 0.25, 0.50, 0.75, 1.00, 2.00, 3.00, 4.00 and 5.00 h. Peaks with parenthesis and (*) indicate the Bi-2212 and Bi-2201 peaks, respectively



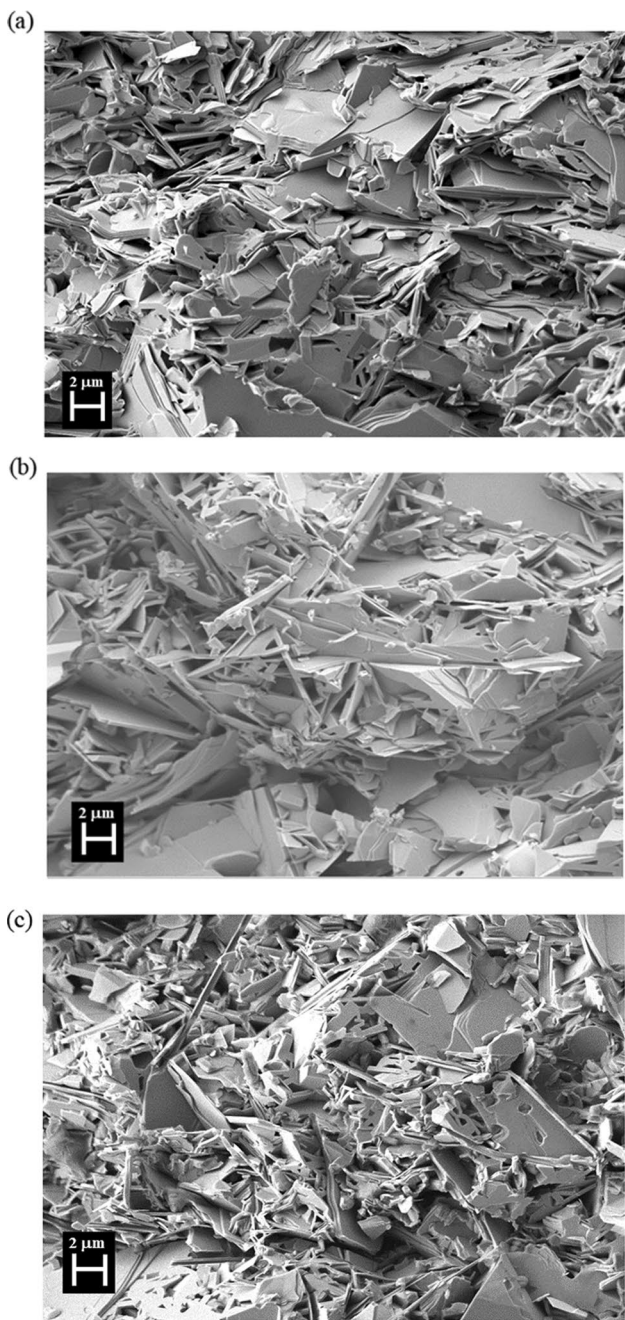


Fig. 4 FESEM micrographs of **a** non-irradiated $(\text{Bi}_{1.6}\text{Pb}_{0.4})\text{Sr}_2\text{Ca}_2\text{Cu}_3\text{O}_{10}$, **b** sample irradiated for 2 h in DT facility and **c** sample irradiated for 2 h in RR facility

weight percent from $(\text{Bi}_{1.6}\text{Pb}_{0.4})\text{Sr}_2\text{Ca}_2\text{Cu}_3\text{O}_{10}$ composition in all samples. This was probably due to the limitation of EDX to measure light element such as oxygen. Furthermore, peaks representing Zn were observed in all irradiated samples and peak from Po was detected in sample

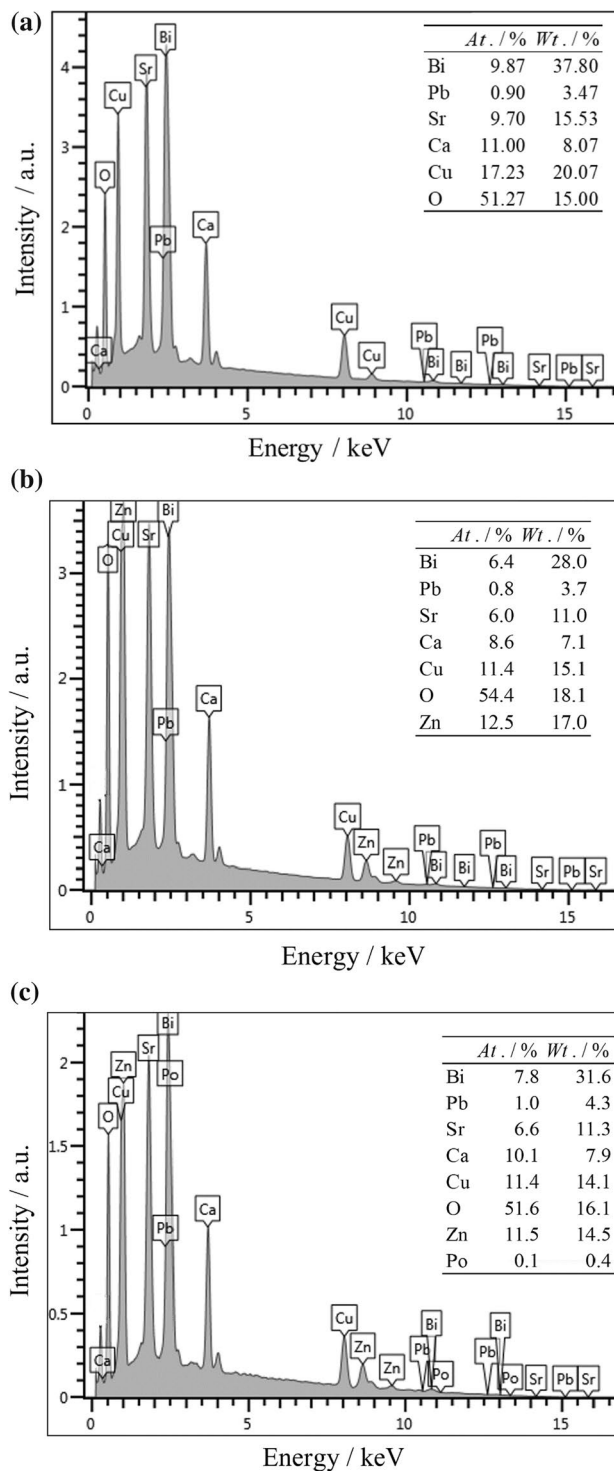


Fig. 5 EDX spectra of **a** non-irradiated $(\text{Bi}_{1.6}\text{Pb}_{0.4})\text{Sr}_2\text{Ca}_2\text{Cu}_3\text{O}_{10}$, **b** sample irradiated for 2 h in DT facility and **c** sample irradiated for 2 h in RR facility. Inset shows the atomic and weight percentage of corresponding elements

irradiated for 2 h in DT facility. The emergence of new elements was due to neutron activation after irradiation.

3.4 Neutron activation

The Neutron Activation and Scattering Calculator was used to estimate the neutron activation of elements for $(\text{Bi}_{1.6}\text{Pb}_{0.4})\text{Sr}_2\text{Ca}_2\text{Cu}_3\text{O}_{10}$ (Table 1) irradiated for 5 h in DT and RR facilities. The calculation was based on 180 days after neutron irradiation. ^{63}Cu interacts with neutrons to produce ^{64}Cu , which then beta decayed to produce a stable nuclide ^{64}Zn . The major contribution of total radioactivity in irradiated $(\text{Bi}_{1.6}\text{Pb}_{0.4})\text{Sr}_2\text{Ca}_2\text{Cu}_3\text{O}_{10}$ is ^{85}Sr , which is the product reaction with neutron activated from ^{84}Sr . Peaks in EDX spectra corresponding to Zn and Po were most likely ^{64}Zn from Cu, and Po-210 from Bi, respectively.

3.5 Gamma spectroscopy

The gamma spectroscopy was performed 180 days after neutron irradiation. Gamma peak energy analysis revealed the

Table 1 Radioactive decay of each element in the $(\text{Bi}_{1.6}\text{Pb}_{0.4})\text{Sr}_2\text{Ca}_2\text{Cu}_3\text{O}_{10.6}$ irradiated samples for 2 h in DT and RR facilities

Element	Nuclide	Half-life, $T_{1/2}$	Activity (μCi)	
			DT; 2.00 h; 4.97×10^{16} n cm^{-2}	RR; 2.00 h; 1.98×10^{16} n cm^{-2}
^{209}Bi	^{210}Bi	3,500,000 years	2.2629×10^{-7}	9.0188×10^{-8}
^{209}Bi	^{210}Po	138.38 days	3.5876×10^{-3}	1.4298×10^{-3}
^{204}Pb	^{205}Pb	14,000,000 years	6.9971×10^{-9}	2.7887×10^{-9}
^{84}Sr	^{85}Sr	64.9 days	2.1773×10^{-1}	8.6775×10^{-2}
^{88}Sr	^{90}Sr	29 years	8.8344×10^{-11}	1.4033×10^{-11}
^{40}Ca	^{41}Ca	130,000 years	1.5963×10^{-4}	6.3621×10^{-5}
^{63}Cu	^{64}Cu	12.7 h	0	0
^{64}Cu	^{64}Zn	Stable	0	0
^{17}O	^{14}C	5736 years	3.9179×10^{-6}	1.5615×10^{-6}

Table 2 Radionuclides of $(\text{Bi}_{1.6}\text{Pb}_{0.4})\text{Sr}_2\text{Ca}_2\text{Cu}_3\text{O}_{10.6}$ irradiated samples in DT and RR facilities for 2 h

Sample	Nuclide	Energy (keV)	Net Area Count (keV cts s^{-1})	Intensity (cts s^{-1})	Uncertainty (%)	FWHM (keV)
Dry tube						
2.00 h; 4.97×10^{16} n cm^{-2}	^{109}Cd	88.04	4574	0.212	9.59	1.337
	^{85}Sr	513.99	352,699	16.329	0.18	1.591
	^{60}Co	1173.08	14,824	0.686	1.32	1.946
	^{60}Co	1332.34	13,906	0.644	1.28	2.030
Rotary rack						
2.00 h; 1.98×10^{16} n cm^{-2}	^{109}Cd	88.04	3484	0.161	12.07	1.337
	^{85}Sr	513.99	155,215	7.186	0.28	1.591
	^{60}Co	1173.12	14,088	0.652	1.35	1.896
	^{60}Co	1332.33	13,008	0.602	1.25	2.077

presence of radionuclide ^{109}Cd , ^{85}Sr and ^{60}Co in samples irradiated for 5 h in DT and RR facilities. Background measurements confirmed that ^{60}Co and ^{51}Cr originated from the laboratory. ^{60}Co peaks at 1173.08 and 1332.34 keV is a common calibration source in many laboratories. It has a half-life of 5.27 years and is synthesized by neutron activation of ^{59}Co . ^{109}Cd has a half-life of 462.6 days and emits gamma rays with a maximum energy of 127 keV. In other hand, ^{85}Sr is the product reaction with neutron activated from ^{84}Sr in $(\text{Bi}_{1.6}\text{Pb}_{0.4})\text{Sr}_2\text{Ca}_2\text{Cu}_3\text{O}_{10.6}$ sample. The intensity of ^{85}Sr at 513.99 keV was the highest in both samples indicating that ^{85}Sr as the main contribution of the total radioactivity in irradiated Bi-2223 (Table 2). This result agrees with Neutron Activation and Scattering Calculator estimation.

3.6 Electrical resistance

The temperature-dependence resistance curves of non-irradiated $(\text{Bi}_{1.6}\text{Pb}_{0.4})\text{Sr}_2\text{Ca}_2\text{Cu}_3\text{O}_{10}$ and samples irradiated in DT facility for 0.25, 0.50, 0.75, 1.00, 2.00, 3.00, 4.00 and 5.00 h are shown in Fig. 6. The onset transition temperature, $T_{\text{c-onset}}$ is defined as the temperature at which a sudden drop in electrical resistivity is first observed. The zero transition temperature, $T_{\text{c-zero}}$ is the temperature at which resistivity is zero. $T_{\text{c-onset}}$ and $T_{\text{c-zero}}$ are indicated in the inset of Fig. 6a. All samples showed the metallic normal-state behavior above the onset transition temperature, $T_{\text{c-onset}}$. $T_{\text{c-onset}}$ and zero transition temperature, $T_{\text{c-zero}}$ for all irradiated samples in DT facility were between 112 and 115 K, and 103 and 105 K, respectively. Figure 7 shows the electrical resistance versus temperature curves of samples irradiated in RR facility for 0.25, 0.50, 0.75, 1.00, 2.00, 3.00, 4.00 and 5.00 h. The metallic normal-state behavior was observed for all irradiated samples in RR facility. $T_{\text{c-onset}}$ and $T_{\text{c-zero}}$ for all irradiated samples in DT facility were between 112 and 116 K, and 100 and 104 K, respectively. Sample irradiated for 1.00 h with neutron fluence of 9.90×10^{15} n cm^{-2}

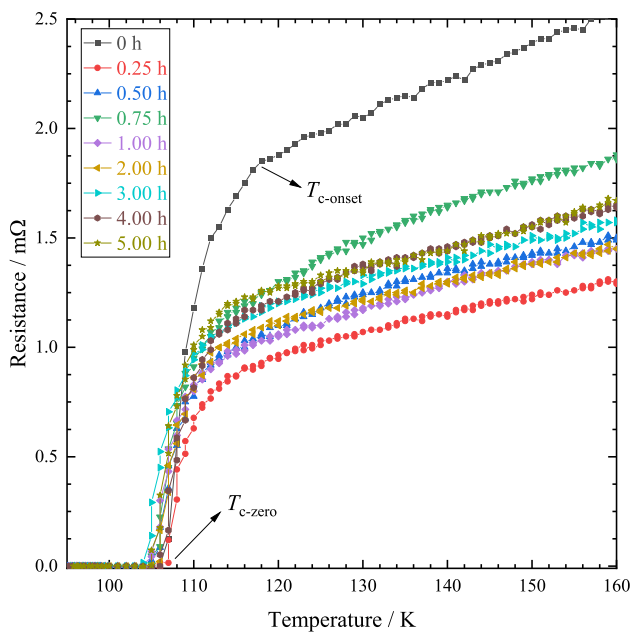


Fig. 6 Electrical resistance versus temperature of non-irradiated $(\text{Bi}_{1.6}\text{Pb}_{0.4})\text{Sr}_2\text{Ca}_2\text{Cu}_3\text{O}_{10}$ and samples irradiated in DT facility for 0.25, 0.50, 0.75, 1.00, 2.00, 3.00, 4.00 and 5.00 h

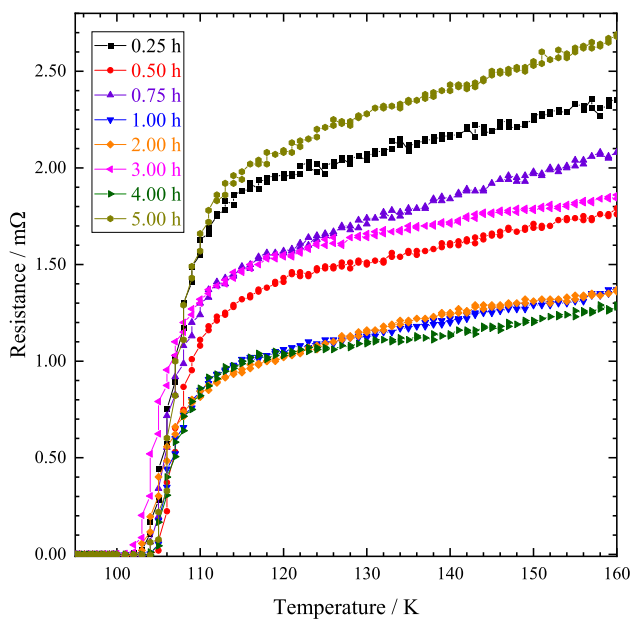


Fig. 7 Electrical resistance versus temperature of $(\text{Bi}_{1.6}\text{Pb}_{0.4})\text{Sr}_2\text{Ca}_2\text{Cu}_3\text{O}_{10}$ irradiated in RR facility for 0.25, 0.50, 0.75, 1.00, 2.00, 3.00, 4.00 and 5.00 h

exhibited double onset transition temperatures which were 116 K and 112 K. This is because of the decoupling of the superconducting grains after irradiation [23] and the existence of the impurities phase such as Bi-2212 phase.

The electrical resistance versus temperature curves for all irradiated samples in both facilities showed that the neutron irradiation suppressed the transition temperature of $(\text{Bi}_{1.6}\text{Pb}_{0.4})\text{Sr}_2\text{Ca}_2\text{Cu}_3\text{O}_{10}$ as well as Bi-2223 phase. This can be explained in term of carrier concentration. Neutron can penetrate into the crystal lattice and displace the oxygen atoms, which are located in small point defects (oxygen vacancies) [11]. The displacement of oxygen, which is important in cuprate carrier behavior, resulted in the suppression of the transition temperature of $(\text{Bi}_{1.6}\text{Pb}_{0.4})\text{Sr}_2\text{Ca}_2\text{Cu}_3\text{O}_{10}$. In addition, new elements such as Zn may also have contributed to the change in carrier concentration. Furthermore, the formation of the Bi-2212 phase can be associated with the decrease in T_c . For example, with increasing neutron fluence in the DT facility, $T_{c\text{-onset}}$ generally decreased between 115 and 114 K while the volume fraction of the Bi-2212 phase increased between 37 and 64%. This implied that the increased formation of Bi-2212 phase could have contributed to the suppression of the T_c .

The transition temperatures, after irradiation were nearly plateaued, mainly for samples irradiated in the DT facility. This indicated that increasing the exposure time and neutron fluence had no significant effect on the carrier concentration of $(\text{Bi}_{1.6}\text{Pb}_{0.4})\text{Sr}_2\text{Ca}_2\text{Cu}_3\text{O}_{10}$. Furthermore, the deviation of $T_{c\text{-onset}}$ and $T_{c\text{-zero}}$ among all irradiated samples in DT facility were smaller and more systematic than irradiated samples in RR facility. This pattern was also observed in the volume fraction of Bi-2223 phase. The location of the facilities could be one explanation for these results. DT are empty tubes located in core position in the reactor. As a result, there is less moderation process that may disrupt the distribution of neutrons. Meanwhile, RR facility is in the graphite reflector which undergoes moderation process such as thermalization [20]. Moreover, despite the RR facility is a rotating system, the shape of container was not precisely parallel to the length axis of the fuel elements. Hence, some space existed between the container and the inner side of the irradiation tube, contributing to neutron flux distribution inhomogeneity [19, 24]. Therefore, neutron distribution in DT facility is more uniform compared with RR facility.

The electrical resistivity at room temperature for all samples are presented in Table 3. The resistivity at room temperature for non-irradiated sample was 5.05 mΩ cm. In general, neutron irradiation decreased the resistivity at room temperature, $\rho_{297\text{K}}$ for all samples in both DT and RR facilities. There were no systematic changes in $\rho_{297\text{K}}$ for irradiated samples in both facilities. These results are consistent with a previous study that found a similar behavior of electrical resistivity of Bi-2223 at room temperature for low energy neutron irradiation [13]. This is because neutron irradiation destroyed the weak linked between the grains [13]. This also suggested that neutron irradiation is an effective

Table 3 Neutron fluence, $T_{c-onset}$, T_{e-zero} , $\rho_{297\text{K}}$, lattice parameters for Bi-2223 phase, volume fraction V_{2223} , V_{2212} and V_{2201} , T_{cx} , T_{pl} , T_{pH} , $J_{c-t}(50\text{ K})$, $J_{c-t}(77\text{ K})$ of non-irradiated ($\text{Bi}_{1.6}\text{Pb}_{0.4}$) $\text{Sr}_2\text{Ca}_2\text{Cu}_3\text{O}_{10}$ and samples irradiated for 0.25, 0.50, 0.75, 1.00, 2.00, 3.00, 4.00 and 5.00 h in DT and RR facilities

Irradiation time (h)	Neutron Fluence (n cm^{-2})	$T_{c-onset}$ (K)	T_{e-zero} (K)	$\rho_{297\text{K}}$ ($\text{m}\Omega\text{-cm}$)	a (\AA)	c (\AA)	V (\AA^3)	V_{2223} (%)	V_{2212} (%)	V_{2201} (%)	T_{cx} (K)	T_{pH}/T_{pl} (K)	$J_{c-t}(50\text{ K})$ (A cm^{-2})	$J_{c-t}(77\text{ K})$ (A cm^{-2})
Dry tube														
0	0	118	105	5.05	5.406	37.134	1085.38	85	12	3	108	96	2.14	1.63
0.25	6.21×10^{15}	115	105	2.74	5.406	37.203	1087.15	62	38	1 <	109	97	2.35	0.91
0.50	1.24×10^{16}	113	104	3.08	5.402	37.150	1084.16	50	50	0	107	106/95	2.82	1.60
0.75	1.86×10^{16}	112	104	3.03	5.395	37.121	1080.41	43	57	0	109	98	3.06	0.88
1.00	2.48×10^{16}	113	103	3.11	5.396	37.169	1081.28	46	54	0	107	105/95	10.70	8.23
2.00	4.97×10^{16}	114	103	3.38	5.406	37.167	1086.31	56	43	1	107	104/93	2.12	1.71
3.00	7.45×10^{16}	113	103	3.10	5.398	37.126	1081.61	36	64	0	106	104/94	4.19	3.01
4.00	9.94×10^{16}	113	104	3.21	5.400	37.145	1082.96	55	45	0	107	105/96	14.41	5.70
5.00	1.24×10^{17}	114	103	3.91	5.401	37.171	1084.25	63	37	0	106	104/96	0.54	0.40
Rotary rack														
0.25	2.48×10^{15}	116	101	5.31	5.410	37.274	1091.08	33	27	0	105	103/85	1.96	1.58
0.50	4.95×10^{15}	115	104	3.55	5.395	37.151	1081.14	54	46	0	105	103/93	4.74	2.70
0.75	7.43×10^{15}	112	103	3.70	5.398	37.188	1083.45	41	59	0	105	103/93	6.44	3.40
1.00	9.90×10^{15}	112/116	103	2.53	5.421	37.156	1091.83	75	25	0	109	107/97	6.69	5.82
2.00	1.98×10^{16}	114	100	1.93	5.395	37.171	1081.78	55	45	1 <	105	103/94	7.57	6.11
3.00	2.97×10^{16}	112	100	3.12	5.421	37.119	1090.94	71	29	0	108	106/96	9.80	8.43
4.00	3.96×10^{16}	117	103	2.30	5.405	37.185	1086.38	74	26	1 <	105	103/94	15.88	13.59
5.00	4.95×10^{16}	112	103	4.65	5.396	37.172	1082.24	20	80	0	105	103/88	3.78	3.13

method for lowering the normal state resistivity of Bi-2223 superconductors.

3.7 AC susceptibility

The complex AC susceptibility ($\chi = \chi' + i\chi''$) measurement of non-irradiated $(\text{Bi}_{1.6}\text{Pb}_{0.4})\text{Sr}_2\text{Ca}_2\text{Cu}_3\text{O}_{10}$ and samples irradiated in DT facility for 0.25, 0.50, 0.75, 1.00, 2.00, 3.00, 4.00 and 5.00 h are shown in Fig. 8. The real part of susceptibility χ' is associated with the diamagnetic behavior, whereas the imaginary part of susceptibility, χ'' shows the nature of flux pinning strength and grain connectivity. A sudden deviation from straight line in χ' denotes the susceptibility transition temperatures, $T_{c\chi'}$ or the onset of transition temperature for bulk superconductivity. $T_{c\chi'}$ also signifies the beginning of the magnetic shielding. Two peaks in χ'' that represent AC losses should be observed. The first small peak at higher temperatures T_{pH} is associated with intrinsic losses while the second pronounced peak at lower temperatures is related to intergranular current density, J_{cs} . The temperature at the second pronounced peak in χ'' , T_{pL} is correlated with flux pinning strength and intergranular coupling.

In general, our AC susceptibility measurements revealed feebly visible intrinsic losses peaks between 104 and 106 K for irradiated samples. This indicated the presence of weak coupling among the grains which weakened the interaction between neighboring Bi-2223 superconducting grains as a result of microstructure defects caused by neutron irradiation. The $T_{c\chi'}$ for non-irradiated sample was 108 K. The highest $T_{c\chi'}$ was 109 K for samples irradiated

for 0.25 and 0.75 h in DT facility. $T_{c\chi'}$ for other irradiated samples was between 106 and 107 K. The highest T_{pL} (98 K) recorded was for sample irradiated for 0.75 h with fluence of $1.86 \times 10^{16} \text{ n cm}^{-2}$ indicating that the enhancement of flux pinning energy and intergranular coupling. There were no systematic change in T_{pL} and T_{pH} for all irradiated samples in DT facility. Besides that, T_{pH} was not observed in samples irradiated for 0.25 and 0.75 h. T_{pH} may be obscured with T_{pL} due to the strong coupling between the grains in these irradiated samples. This also demonstrated that the grain coupling took place immediately after the occurrence of superconductivity within the grains [25].

For all irradiated samples in RR facility, the AC susceptibility curves are shown in Fig. 9. All irradiated samples showed a barely discernible intrinsic losses peak in imaginary part of χ at around 103 to 107 K (see supplementary data). The highest $T_{c\chi'}$ and T_{pL} were 109 K and 97 K, respectively for samples irradiated for 1.00 h in RR facility. In general, other irradiated samples showed a decreased of $T_{c\chi'}$ and T_{pL} and T_{pH} as compared with non-irradiated sample.

In both DT and RR facilities, the $T_{c\chi'}$ and T_{pL} and T_{pH} generally decreased after irradiation, indicating that the suppressing of flux pinning energy and weakening of intergranular coupling after neutron irradiation. This was consistent with SEM characterization, which revealed the presence of smaller grains size in the sample irradiated for 2 h (Fig. 4b, c). However, at specific irradiation time and neutron fluence (in our case, 0.25 and 0.50 h irradiation in DT facility and 1.00 h irradiation for RR facility), the flux pinning strength and intergranular coupling were enhanced. Besides that, the

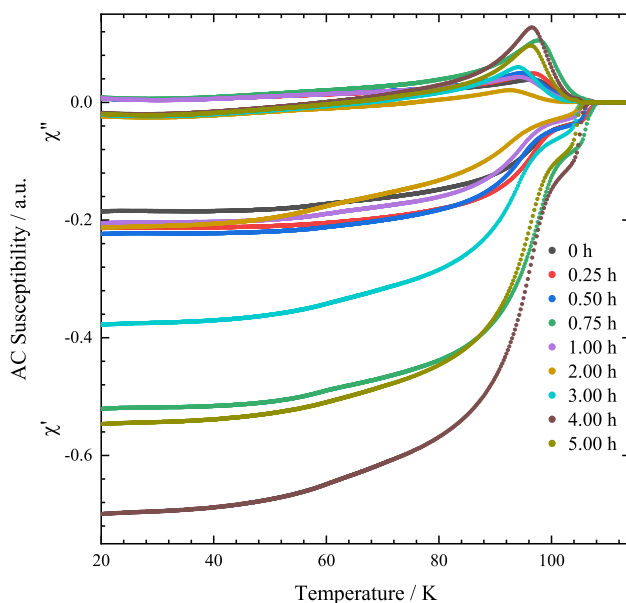


Fig. 8 AC susceptibility ($\chi = \chi' + i\chi''$) versus temperature of non-irradiated $(\text{Bi}_{1.6}\text{Pb}_{0.4})\text{Sr}_2\text{Ca}_2\text{Cu}_3\text{O}_{10}$ and samples irradiated in DT facility for 0.25, 0.50, 0.75, 1.00, 2.00, 3.00, 4.00 and 5.00 h

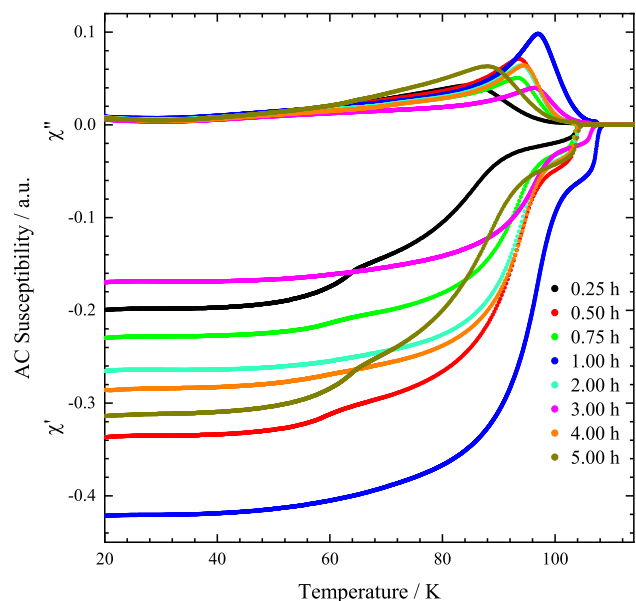


Fig. 9 AC susceptibility ($\chi = \chi' + i\chi''$) versus temperature of $(\text{Bi}_{1.6}\text{Pb}_{0.4})\text{Sr}_2\text{Ca}_2\text{Cu}_3\text{O}_{10}$ irradiated in RR facility for 0.25, 0.50, 0.75, 1.00, 2.00, 3.00, 4.00 and 5.00 h

reduction in $T_{c\chi}$, T_{pL} and T_{pH} were more prominent for samples irradiated in the RR facility compared to DT facility.

3.8 Critical current density

The transport critical current density, J_{c-t} versus temperature for non-irradiated $(\text{Bi}_{1.6}\text{Pb}_{0.4})\text{Sr}_2\text{Ca}_2\text{Cu}_3\text{O}_{10}$ and samples irradiated in DT facility for 0.25, 0.50, 0.75, 1.00, 2.00, 3.00, 4.00 and 5.00 h are shown in Fig. 10. J_{c-t} was measured via the four probe method using $1 \mu\text{V}/\text{cm}$. The non-irradiated sample showed $J_{c-t} = 2.14 \text{ A cm}^{-2}$ at 50 K. J_{c-t} at 50 K increased as irradiation time increased up until 1.00 h irradiation time. Then, J_{c-t} decreased until 3.00 h irradiation time. The highest J_{c-t} at 40 K was for sample irradiated for 4.00 h with neutron fluence of $9.94 \times 10^{16} \text{ n cm}^{-2}$ which was 14.41 A cm^{-2} . Neutron exposure for 5.00 h with $1.24 \times 10^{17} \text{ n cm}^{-2}$ fluence severely suppressed J_{c-t} . This also indicated that substantially higher neutron fluence ($10^{17} \text{ n cm}^{-2}$) destroyed the flux pinning and current density of Bi-2223 phase superconductor.

The transport critical current density, J_{c-t} versus temperature for all irradiated samples in RR facility are shown in Fig. 11. For 0.25 h irradiation time, J_{c-t} at 50 K decreased from 2.14 A cm^{-2} to 1.96 A cm^{-2} . Then, J_{c-t} increased as irradiation time and neutron fluence increased except for 5.00 h irradiation time. The highest J_{c-t} (15.88 A cm^{-2}) at 40 K was for sample irradiated for 4.00 h with neutron fluence of $4.95 \times 10^{16} \text{ n cm}^{-2}$.

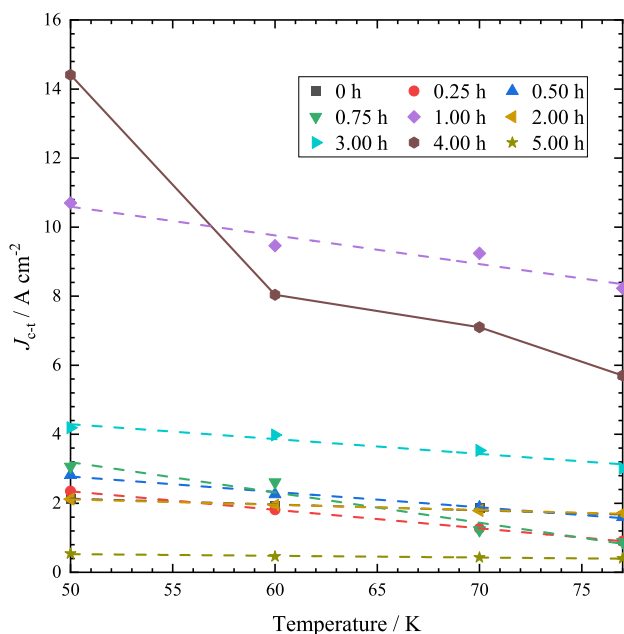


Fig. 10 J_{c-t} versus temperature of non-irradiated $(\text{Bi}_{1.6}\text{Pb}_{0.4})\text{Sr}_2\text{Ca}_2\text{Cu}_3\text{O}_{10}$ and samples irradiated in DT facility for 0.25, 0.50, 0.75, 1.00, 2.00, 3.00, 4.00 and 5.00 h

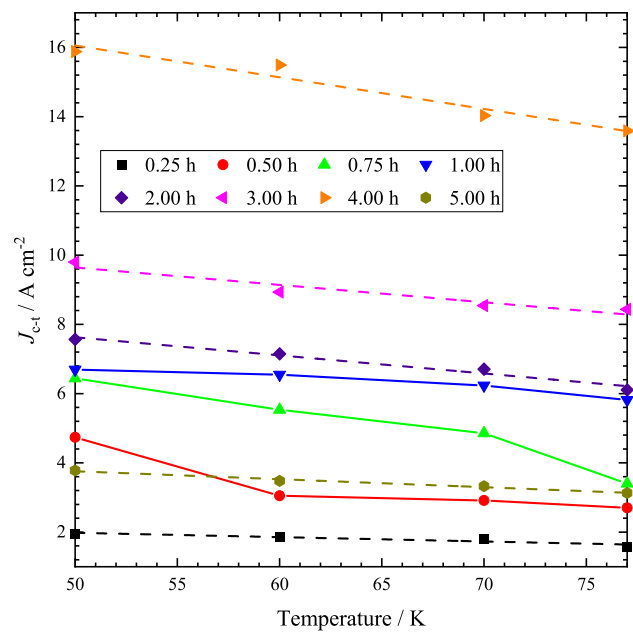


Fig. 11 J_{c-t} versus temperature of $(\text{Bi}_{1.6}\text{Pb}_{0.4})\text{Sr}_2\text{Ca}_2\text{Cu}_3\text{O}_{10}$ irradiated in RR facility for 0.25, 0.50, 0.75, 1.00, 2.00, 3.00, 4.00 and 5.00 h

In general, irradiated samples in both DT and RR facilities showed remarkably enhanced transport critical current density except for samples irradiated for 5.00 h in DT and RR facilities, respectively. Although the transition temperatures were suppressed more pronouncedly in RR than in the DT facility, the RR facility demonstrated better enhancement of J_{c-t} . In terms of neutron fluence, it is proposed that neutron fluences ranging from 2.48×10^{16} to $3.96 \times 10^{16} \text{ n cm}^{-2}$ are optimal to increase J_{c-t} in the $(\text{Bi}_{1.6}\text{Pb}_{0.4})\text{Sr}_2\text{Ca}_2\text{Cu}_3\text{O}_{10}$ superconductor.

Based on self-field approximation and J_{c-t} dependence on temperature between 50 and 77 K [26, 27], the correlation between characteristic length, L_c associated with the pinning force and the average grain size, R_g can be determined. A linear decrease in J_{c-t} was exhibited for all samples irradiated in DT facility except for sample irradiated for 4.00 h. The linear drop of J_{c-t} signifies that the characteristic length, L_c is almost the same as the average grain size, R_g ($L_c \sim R_g$). The non-linear decrease showed by sample irradiated for 4.00 h implied that the L_c is smaller than R_g ($L_c < R_g$).

For irradiated samples in RR facility, the curves shown by samples irradiated for 0.75 and 1.00 h indicated that L_c is larger than R_g ($L_c > R_g$). As shown in Fig. 11, samples that were irradiated for a longer period and with a higher neutron fluence showed a linear decrease in J_{c-t} versus temperature, indicating that $L_c \sim R_g$. The various curves behavior implies that different pinning mechanism has taken place after neutron irradiation in both facilities. Neutron fluence, $T_{c-\text{onset}}$, $T_{c-\text{zero}}$, $\rho_{297 \text{ K}}$, lattice parameters for Bi-2223 phase, volume fraction V_{2223} , V_{2212} and V_{2201} , $T_{c\chi}$, T_{pL} , T_{pH} , $J_{c-t}(50 \text{ K})$ and

J_{c-1} (77 K) of non-irradiated $(\text{Bi}_{1.6}\text{Pb}_{0.4})\text{Sr}_2\text{Ca}_2\text{Cu}_3\text{O}_{10}$ and samples irradiated in DT and RR facilities are presented in Table 3.

4 Conclusion

The effect of neutron irradiation in dry tube (DT) and rotary rack (RR) facilities on the superconducting properties of $(\text{Bi}_{1.6}\text{Pb}_{0.4})\text{Sr}_2\text{Ca}_2\text{Cu}_3\text{O}_{10}$ (Bi-2223) have been studied. The neutron irradiation resulted in the enhancement of critical current density although the transition temperatures and Bi-2223 phase formation were suppressed. Sample irradiated for 4.0 h with neutron fluence of $3.96 \times 10^{16} \text{ n cm}^{-2}$ in the RR facility showed the highest J_{c-1} (15.88 A cm^{-2}) at 50 K. J_{c-1} for samples irradiated in the RR facility was higher than samples irradiated in the DT facility. An appropriate irradiation time and neutron fluence optimized the peak temperature of imaginary susceptibility indicating that the enhancement of flux pinning strength and intergranular coupling. Our results showed that the optimum neutron fluence were between 2.48×10^{16} and $3.96 \times 10^{16} \text{ n cm}^{-2}$. These findings can be useful in determining the optimized irradiation time and neutron fluence as well as appropriate irradiation facilities to improve the superconducting properties of Bi-2223. Other works, such as neutron irradiation in out-core facilities with different irradiation time and neutron fluence are interesting areas for future research. The Bi-2223 phase in other forms such as tapes and thin films normally have higher J_c than in the pellet form. Hence, samples in the tapes and thin films form can also be prepared and irradiated with neutron using the optimal condition found in this work to improve the critical current density in future studies.

Acknowledgements The authors thank the Universiti Tenaga National through UNITEN BOLD Publication Fund (J510050002-IC-6 BOLDREFRESH2025) and Yayasan Canselor UNITEN (no. 202210021YCU) and the Ministry of Higher Education, Malaysia (no. FRGS/1/2020/STG07/UKM/01/1) for the funding.

Author contribution Conceptualization: MM, RA-S; methodology: ABPI, NAH; formal analysis and investigation: KM-N, RA; writing—original draft preparation: MM; writing—review and editing: RA-S; funding acquisition: MM, RA-S; resources: FMI, AMJB, NSH, supervision: RA-S.

Data availability Data are available from the corresponding author upon reasonable request.

Declarations

Conflict of interest The authors declare that they have no relevant financial or non-financial interests to disclose. The authors also declare they have no competing interests to declare that are relevant to the content of this article. All authors certify that they have no affiliations with or involvement in any organization or entity with any financial interest or non-financial interest in the subject matter or materials discussed in

this manuscript. The authors also declare that they have no financial or proprietary interests in any material discussed in this article.

References

1. J. Takada, H. Kitaguchi, T. Egi, K. Oda, Y. Miura, H. Mazaki, Y. Ikeda, Z. Hiroi, M. Takano, Y. Tomii, *Phys. C* **170**, 3 (1990)
2. M. Ismail, R. Abd-Shukor, I. Hamadne, S.A. Halim, J. Mater. Sci. **39**, 10 (2004)
3. N.R. Mohd Suib, I.P. Abu Bakar, N.B. Ibrahim, R. Abd-Shukor, *J. Supercond. Nov. Magn.* **32**, 2 (2019)
4. W. Kong, R. Abd-Shukor, *J. Supercond. Nov. Magn.* **23**, 2 (2010)
5. M. Hafiz, R. Abd-Shukor, *Adv. Mater. Sci. Eng.* **2015**, 146476 (2015)
6. M. Roumié, S. Marhaba, R. Awad, M. Kork, I. Hassan, R. Mawassi, *J. Supercond. Nov. Magn.* **27**, 1 (2014)
7. A. Agail, R. Abd-Shukor, *J. Supercond. Nov. Magn.* **27**, 5 (2014)
8. I.F. Lyuksyutov, D.G. Naugle, *Mod. Phys. Lett. B* **13**, 15 (1999)
9. I.H. Gul, F. Amin, A.Z. Abbasi, M. Anis-ur-Rehman, A. Maqsood, *Phys. C* **449**, 2 (2006)
10. C.S. Pande, *Mater. Phys. Mech.* **2**, 1 (2000)
11. M.A. Ali, K.A. Jasim, *Energy Proc.* **157**, 879–891 (2019)
12. T. Shitamichi, M. Nakano, T. Terai, M. Yamawaki, T. Hoshiya, *Phys. C* **392–396**, 254–258 (2003)
13. W.M. Chen, S.S. Jiang, Y.C. Guo, J.R. Jin, X.S. Wu, X.H. Wang, X. Jin, X.N. Xu, X.X. Yao, S.X. Dou, *Phys. C* **299**, 1–2 (1998)
14. Q.Y. Hu, H.W. Weber, F.M. Sauerzopf, G.W. Schulz, R.M. Schalk, H.W. Neumüller, S.X. Dou, *Appl. Phys. Lett.* **65**, 23 (1994)
15. T. Aoki, H. Ueda, A. Ishiyama, N. Miyahara, N. Kashima, S. Nagaya, *IEEE Trans. Appl. Supercond.* **21**, 3 (2011)
16. M. Akamatsu, H. Ikeda, R. Yoshizaki, T. Iwaia, in *Advances in Superconductivity V*, ed. By Y. Bando, H. Yamauchi (Springer, Tokyo 1993), p. 439
17. J.G. Ossandon, J.R. Thompson, Y.C. Kim, Y.R. Sun, D.K. Christen, B.C. Chakoumakos, *Phys. Rev. B* **51**, 13 (1995)
18. S.D. Moss, W.G. Wang, S.X. Dou, R. Weinstein, *INIS* **29** (1998)
19. A.R. Yavar, S. Sarmani, A.K. Wood, S.M. Fadzil, Z. Masood, K.S. Khoo, *Radiat. Meas.* **46**, 2 (2011)
20. M.H. Rabir, J. Abdul Karim, M.R. Mohamed Zin, *Jurnal Sains Nuklear Malaysia* **29**, 2 (2017)
21. I.A. Alnour, H. Wagiran, N. Ibrahim, S. Hamzah, B.S. Wee, M.S. Elias, J.A. Karim, *J. Radioanal. Nucl. Chem.* **296**(296), 3 (2013)
22. R.B. Beyers, S.S.P. Parkin, V.Y. Lee, A.I. Nazzal, R.J. Savoy, G.L. Gorman, T.C. Huang, S.J.L. Placa, *IBM J. Res. Dev.* **33**, 3 (1989)
23. E. Hannachi, Y. Slimani, A. Ekicibil, A. Manikandan, F.B. Azzouz, *Mater. Chem. Phys.* **235**, 121721 (2019)
24. K. Khoo, S. Sarmani, I. Abugassa, *J. Radioanal. Nucl. Chem.* **271**, 2 (2007)
25. I.P.A. Bakar, K. Muhammad-Aizat, J. Nur-Akasyah, M.S. Mohd-Syahmi, N.R. Mohd Suib, W.S. Chiu, R. Abd-Shukor, *Appl. Phys. A* **125**, 1 (2018)
26. A. Kilic, *Supercond. Sci. Technol.* **8**, 7 (1995)
27. A. Kilic, K. Kilic, S. Senoussi, *J. Appl. Phys.* **84**, 6 (1998)

Publisher's Note Springer Nature remains neutral with regard to jurisdictional claims in published maps and institutional affiliations.

Springer Nature or its licensor (e.g. a society or other partner) holds exclusive rights to this article under a publishing agreement with the author(s) or other rightsholder(s); author self-archiving of the accepted manuscript version of this article is solely governed by the terms of such publishing agreement and applicable law.